Steel and Composite Structures, *Vol. 20, No. 1 (2016) 147-166*
DOI: http://dx.doi.org/10.12989/scs.2016.20.1.147

Stability analyses of a cylindrical steel silo with corrugated sheets and columns

Mateusz Sondej [a], Piotr Iwicki, Michał Wójcik and Jacek Tejchman [*]

Department of Civil and Environmental Engineering, Gdańsk University of Technology, Narutowicza 11/12, 80-233 Gdańsk, Poland

(*Received November 08, 2014, Revised July 06, 2015, Accepted September 11, 2015*)

Abstract. The paper presents comprehensive quasi-static stability analysis results for a real funnel-flow cylindrical steel silo composed of horizontally corrugated sheets strengthened by vertical thin-walled column profiles. Linear buckling and non-linear analyses with geometric and material non-linearity were carried out with a perfect and an imperfect silo by taking into account axisymmetric and non-axisymmetric loads imposed by a bulk solid following Eurocode 1. Finite element simulations were carried out with 3 different numerical models (single column on the elastic foundation, 3D silo model with the equivalent orthotropic shell and full 3D silo model with shell elements). Initial imperfections in the form of a first eigen-mode for different wall loads and from 'in-situ' measurements with horizontal different amplitudes were taken into account. The results were compared with Eurocode 3. Some recommendations for the silo dimensioning were elaborated.

Keywords: silo; corrugated sheet; columns; buckling; stability; numerical modelling; Eurocode; geodetic measurements

1. Introduction

Silos are engineering structures widely used in industries and farms to store, feed and process bulk solids that is essential to agricultural, mining, mineral processing, chemical, shipping and other industries (Fayed and Otten 1997, Safarian and Harris 1985). They are mainly built from concrete or metal (steel and aluminium). Metal silos can be built of thin-walled isotropic plain rolled sheets (which can be welded, riveted or screwed around the silo perimeter) or of thin-walled corrugated curved sheets strengthened by vertical stiffeners (columns) distributed uniformly around the silo circumference and connected with screws. Those latter are frequently used in the engineering practice due to an economical steel consumption and a small silo weight. In these silos, it is assumed that horizontally corrugated wall sheets carry circumferential tensile forces caused by horizontal wall pressure and columns carry vertical compressive forces due to the vertical wall friction traction exerted from bulk solids.

A common mechanical failure form in all metal silos is a stability loss caused by the compressive wall friction force due to the interaction between the silo fill and silo wall,

*Corresponding author, Professor, E-mail: tejchmk@pg.gda.pl
[a] Ph.D. Student, E-mail: matsonde@pg.gda.pl

http://www.techno-press.org/?journal=scs&subpage=8 ISSN: 1229-9367 (Print), 1598-6233 (Online)

particularly during eccentric filling and discharge (Brown and Nielsen 1998, Rotter 2001) and dynamic mass flow (Tejchman and Gudehus 1993, Tejchman 1999, Wilde *et al*. 2008). In contrast to many buckling analyses performed for silo shells with isotropic plain rolled thin-walled walls (Brown and Nielsen 1998, Knebel and Schweizerhof 1995, Song and Teng 2003, Sadowski and Rotter 2011), the comprehensive buckling analyses of silos consisted of horizontally corrugated sheets and vertical stiffeners are still in minority (Wójcik *et al*. 2011, Iwicki *et al*. 2011). The treatment of the local buckling within the framework of EN 1993-4-1 (2007) provides 2 alternative procedures to calculate the buckling strength of vertical columns around the silo circumference which significantly differ. In the case of a silo with sparsely distributed columns, the approach in EN 1993-4-1 (2007) is very conservative since it does not take into account a real 3D behaviour of a silo shell containing a silo fill (Wójcik *et al*. 2011). In order to capture more realistically a buckling process in silos, it is advantageous to apply the finite element method which enables to carry out among others linear buckling analyses (LBA), non-linear static analyses or non-linear dynamic analyses. LBA is the simplest analysis, used to estimate critical loads. In turn, non-linear analyses (based on the equilibrium path between the load and displacement) determine the ultimate load by taking into account the effect of the material and geometric characteristics. Sometimes if a static solution is impossible to be achieved due to a convergence loss caused by a localized instability (e.g., surface wrinkling, local buckling or material instability), a dynamic approach has to be applied (Kubiak 2007, Kobayashi *et al*. 2012, Iwicki *et al*. 2014), wherein the time history of a structure response is traced during growing load.

In this paper, the comprehensive static global stability FE analyses were performed for a real steel silo with corrugated walls strengthened by cold-formed open-sectional thin-walled columns by taking initial geometric imperfections into account with a different horizontal amplitude. The FE computations were carried out with the commercial FE package ABAQUS (2010). In the first computation step (model '1'), a single perfect silo column was investigated (in analogy to the solution assumed in EN 1993-4-1 (2007)). Then, a simplified numerical silo model '2' composed of an equivalent orthotropic plate and beam elements representing columns was studied. Finally, in the model '3' 3D shell elements were employed to describe in detail the silo geometry (corrugated wall sheets and columns made from open thin-walled profiles). Advantages and disadvantages of all models were outlined. The results were directly compared with EN 1993-4-1 (2007) for estimating its usefulness in the design practice.

2. Silo characteristics

The real cylindrical metal silo belonging to a silo battery built in Poland was analysed (Wójcik *et al*. 2011). The silo was H = 21.48 m high with the diameter D = 5.35 m (called silo '1'). The cross-section area of the silo was 22.48 m^2 and the perimeter was 16.81 m. The silo walls were made from corrugated steel sheets strengthened with cold-formed open-sectional thin-walled steel profiles fixed to a foundation concrete slab (Fig. 1). The corrugation had the 76 mm pitch and 18 mm depth. The 18 vertical columns distributed uniformly along the silo circumference (at the distance of d_s = 0.93 m) were connected to wall sheets by screws. The outflow took place through a hopper of the height of 2.25 m which was supported on several additional interior columns. The hopper was totally separated from the bin. Its upper part was at the height of 3.44 m above the bin bottom. The silo contained wheat and was designed for funnel flow. The filling and empting process of the silo was concentric.

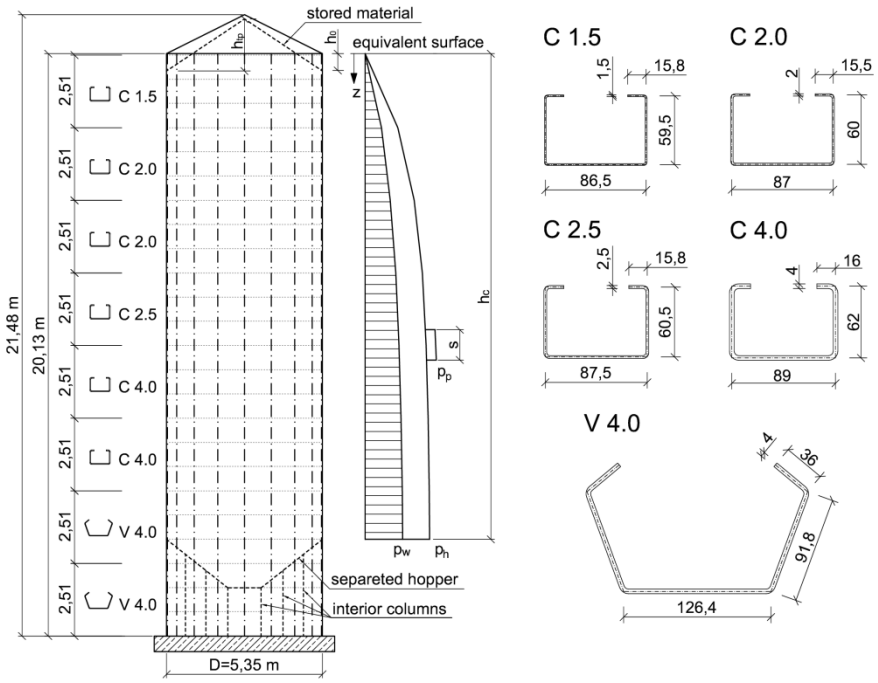

Fig. 1 Geometric silo characteristics, wall friction, normal pressure and patch pressure (p_w, p_h, p_p) and profile cross-sections of silo '1' with corrugated sheets and external vertical columns

The wall pressure due to the stored granular material was calculated using EN 1991-4 (2006). The maximum wall frictional traction and corresponding normal pressure in the bin during emptying were p_w = 13 kPa and p_h = 22 kPa, respectively (at the height of the hopper top). To account for asymmetries (e.g., due to asymmetric filling), the additional patch (local) load p_p over the height of s = 1.05 m was also taken into account (EN 1991-4 2006). A simplified analytical procedure (Gallego *et al*. 2011) was applied for predicting the worst location of the patch load. The maximum horizontal tensile normal stress in thee corrugated sheets was equal to 88 MPa and was significantly smaller than the permissible steel yield stress equal to 350 MPa.

3. Buckling strength according to Eurocode 3

Depending upon the column distance d_s, there exist two alternative buckling approaches in EN 1993-4-1 (2007). The first approach (called 'A') should be used for densely distributed columns

$$d_s < d_{s,\max} = 7.4\left(\frac{r^2 D_y}{C_y}\right)^{0.25}. \tag{1}$$

In this case the critical buckling resultant resistance $n_{x,Rcr}$ per the unit circumference of the orthotropic shell should be evaluated at each appropriate level in the silo by minimising the expression in Eq. (2) with respect to the critical circumference wave number j and the buckling height l_i

$$n_{x,Rcr} = \min\left(\frac{1}{j^2\omega^2}\left(A_1 + \frac{A_2}{A_3}\right)\right), \tag{2}$$

where D_y - the flexural rigidity parallel to the corrugation, C_y - the stretching stiffness parallel to the corrugation and r - the cylinder radius, j - the circumference wave number, ω - the parameter including buckling height l_i and $A_{1,2,3}$ - the parameters including the flexural and stretching stiffness in orthogonal directions of the equivalent orthotropic cylinder (EN 1993-4-1 (2007)). The characteristic buckling resistance $n_{x,Rk}$ for the orthotropic shell should be determined as the smaller value of Eqs. (3) and (4)

$$n_{x,Rk} = \alpha_x n_{x,Rcr}, \tag{3}$$

$$n_{x,Rk} = A_{eff} f_y / d_s, \tag{4}$$

where α_x - the elastic buckling imperfection reduction factor (α_x = 0.8), A_{eff} - the effective cross-sectional area of the stiffener and f_y - the yield stress. Assuming that all vertical loads are carried by stiffeners only, the characteristic buckling resistance per each column is equal to the lower value of Eqs. (5) and (6)

$$N_{b,Rk} = \alpha_x n_{x,Rcr} d_s, \tag{5}$$

$$N_{b,Rk} = A_{eff} f_y \tag{6}$$

The following assumptions were met to lay down Eq. (2):

- the cylindrical shell is loaded by vertical forces prescribed at both ends only (horizontal pressure is not considered),
- the resulting smeared stiffness is uniformly distributed,
- the equivalent shell mid-surface is taken as the central axis of corrugation,
- the cylindrical shell has hinge supports at ends,
- the buckling mode radial displacements are described by the function

$$w = \overline{w} \sin\left(\frac{m\pi x}{L}\right)\cos\left(\frac{ny}{R}\right), \tag{7}$$

where L - the height of the cylinder, m and n - the wave numbers in the x and y direction, R - the radius of the cylinder mid-surface, x - the axial coordinate, y - the circumferential arc-length coordinate.

If the horizontal distance between the columns $d_s > d_{s,\max}$, the buckling resistance should be determined for individual columns using the second approach (called '*B*'):

(*B*1) by ignoring the supporting action of wall sheets in resisting buckling displacements normal to the wall or

(*B*2) by allowing for the stiffness of wall sheets in resisting buckling displacements normal to the wall.

The more realistic method '*B*2' is usually used. The design buckling resistance of a single vertical column in the method '*B*' is given by

$$N_{b,Rk} = 2\sqrt{EI_y K}\,, \tag{8}$$

where EJ_y - the flexural rigidity of the columns in the plane perpendicular to the wall and K - the bending stiffness of the wall sheets between the vertical columns, calculated as

$$K = k_s \frac{D_y}{d_s^3} \tag{9}$$

with the coefficient $k_s = 6$. The wall bending stiffness D_y equals

$$D_y = 0.13Etd^2\,, \tag{10}$$

where E – the modulus of elasticity of the wall, t – the wall thickness and d – the sheet height. The following assumptions were taken into account:

- the 2D behaviour of the column (beam) is considered only,
- the number of buckling half-waves along the circumference is equal to the half of the columns number (if the number of column is a multiple of 4),
- the column is loaded by vertical forces prescribed at both ends only (horizontal pressure is not considered),
- the column is supported at one side by elastic springs simulating the presence of corrugated sheets,
- the column has hinges at ends.

Eq. (8) may be analytically derived from the equilibrium equation for a vertical column supported by an elastic foundation (Wójcik *et al*. 2011).

In the case of the considered silo '1' (with the number of columns n = 18), the distance d_s = 0.933 m is very close to $d_{s,\max}$ = 0.943 m. Thus, two Eurocode approaches ('*A*' and '*B*') may be applied at the same time. Table 1 includes the profile cross-sectional characteristics calculated with the rounded corners (marked as '*rc*') and without them (marked as '*sc*'). The effective cross-section area was calculated including the local and distortional buckling (EN 1993-4-1 2007).

The characteristic maximum normal forces in each profile during silo filling and discharge are listed in Table 2 (calculated according to EN 1991-4 (2006) by taking into account the worst location of the patch load).

The critical buckling resistance $N_{b,rk}$ and load bearing capacity factors are shown in Table 3. The differences between the normal forces calculated with the increased substitute uniform

Table 1 Columns cross-section properties: area and inertia moments ('*rc*'-section with rounded corners and '*sc*'-section with sharp corners

Profile	A_{rc} [cm^2]	A_{eff} [cm^2]	A_{sc} [cm^2]	$J_{y,rc}$ [cm^4]	$J_{y,sc}$ [cm^4]	$J_{z,rc}$ [cm^4]	$J_{z,sc}$ [cm^4]
C1.5	3.50	2.57	3.56	18.7	19.3	46.4	47.5
C2.0	4.66	4.07	4.76	25.1	26.1	62.5	64.5
C2.5	5.84	5.53	6.00	31.9	33.5	79.1	82.2
C4.0	9.39	9.39	9.80	53.1	57.4	130.8	139.1
V4.0	15.11	15.11	15.28	221.5	224.8	709.3	720.5

Table 2 Resultant normal forces in column during filling '*f*' and emptying '*e*' at level '*z*' due to uniform pressure 'N_w', patch load 'N_p' and substitute uniform pressure '$N_{w,u}$' (EN 1991-4 2006)

Profile	z [m]	Filling				Discharge			
		N_{wf} [kN]	N_{pf} [kN]	$N_{wf}+N_{pf}$ [kN]	$N_{wf,u}$ [kN]	N_{we} [kN]	N_{pe} [kN]	$N_{we}+N_{pe}$ [kN]	$N_{we,u}$ [kN]
C1.5	2.51	8	1	9	9	9	2	11	11
C2.0	7.53	49	6	55	57	54	13	67	70
C2.5	10.04	75	9	84	86	82	20	103	107
C4.0	15.06	129	16	146	149	142	37	180	185
V4.0	16.73	148	19	167	170	163	44	206	212

Table 3 Buckling forces according to EN 1993-4-1 (2007): $N_{b,Rk(1)}$ - Eq. (6), $N_{b,Rk(2)}$ - Eq. (5), $N_{b,Rk(3)}$ - Eq. (8) ($N_{b,Ek}$ - discharge force with substitute uniform pressure $N_{we,u}$)

Profile	$N_{b,Rk(1)}$ [kN]	$N_{b,Rk(2)}$ [kN]	$N_{b,Rk(3)}$ [kN]	$N_{b,Ek}/N_{b,Rk(1)}$	$N_{b,Ek}/N_{b,Rk(2)}$	$N_{b,Ek}/N_{b,Rk(3)}$
C1.5	124	444	89	0.13	0.03	0.13
C2.0	167	516	103	0.49	0.14	0.68
C2.5	210	589	117	0.55	0.18	0.91
C4.0	343	779	153	0.56	0.23	1.21
V4.0	535	1047	304	0.40	0.19	0.70

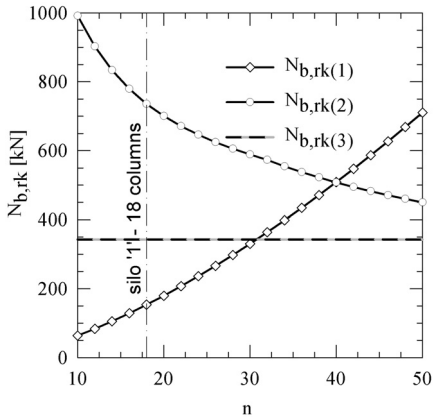

Fig. 2 Change of buckling force $N_{b,rk}$ of single column (C4.0) against column number n ($N_{b,Rk(1)}$ - Eq. (6), $N_{b,Rk(2)}$ - Eq. (5), $N_{b,Rk(3)}$ - Eq. (8))

pressure or with the method considering the worst patch load location are negligible. With an increase of the column number, the stability strength of a single column decreases ($N_{b,rk(2)}$, Eq. (5)) or increases ($N_{b,rk(3)}$, Eq. (8)) (Fig. 2). The buckling force $N_{b,rk(2)}$ in the silo '1' is 5 times higher on average than $N_{b,rk(3)}$ because of an undesired discontinuity between Eqs. (5) and (8) (Fig. 2). The buckling resistance $N_{b,rk(2)}$ is by 270% higher on average than the plastic resistance (including buckling local effects) $N_{b,rk(1)}$ and $N_{b,rk(3)}$ and is by 40% lower on average than $N_{b,rk(1)}$. The strengths by Eqs. (5) and (8) are continuous only for the very high column number n = 40 (Fig. 2). A

significant discrepancy between Eqs. (5) and (8) indicates the weakness of EN 1993-4-1 (2007). Our 3D FE analyses prove that the results with a classical solution of the equivalent orthotropic cylindrical shell (Eq. (2)) produce more realistic results than the a solution based on the single beam resting on the elastic foundation (Eq. (8)).

4. Measured geometric imperfections of real silo

Since the measurements of initial geometric imperfections were not feasible in the considered silo of Section 2 (Fig. 1), we measured them in a similar newly-built cylindrical metal silo with corrugated sheets stiffened by columns (called silo '2'). The silo was 29 m high with the diameter of 15.4 m and included 34 cold-formed open-sectional column profiles at the distance of d_s = 1.4 m. The height of the column was H = 25 m. The corrugation had the 76 mm pitch and 18 mm depth. The silo contained barely. As other similar silos, the silo was built with the use of 17 lifts (Fig. 3(a)) from the top to the bottom. First, the roof was constructed at the ground and in the next steps the silo structure was sequentially lifted (by every second column). During each step the corrugated sheets were assembled (Fig. 3(b)) and the screws were fixed to the sheets. In the final stage, the columns were fixed to the concrete foundation. The applied forces needed for the silo lifting generated some displacements (due to rotations of column joints) which were clearly seen (Fig. 3(c)).

The measurements of column displacements were performed twice: shortly after the silo erection and before the first solid filling and next after the first filling (with 2500 t of barely). The accuracy of displacement measurements was ± 3 mm. The displacements were measured along the silo height every 2.5 m, i.e., between the column connections (Fig. 3(c)). The mean displacements along the silo height before and after filling are presented in Fig. 4(a). The maximum radial displacements of columns varied between − 50 mm (to the silo inside) and + 34 mm (to the silo outside). The shape of the relative mean displacements (Fig. 4(b)) of the wall was in good agreement with the FE calculations. The measured initial radial displacements (shown in Figs. 5(a)-(b) for the empty silo '2') were introduced into the FE model of the silo '1' in Section 2 (18 columns) with the aid of the approximation spline function by keeping the same maximum initial displacements (− 50 mm - + 34 mm). The approximated circumferential imperfections at the height H = 12.5 m are shown in Fig. 5(c). The same technique was used to transfer the measured displacements along the silo height.

(a) silo during erection (b) assembly of corrugated sheets (c) column imperfections

Fig. 3 Erection of silo '2' in Gdańsk (Poland)

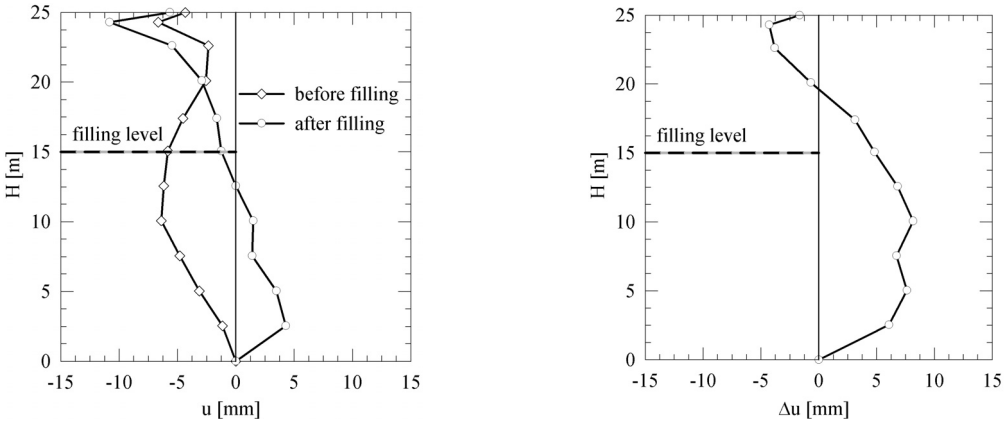

(a) Mean initial radial displacements (b) Relative radial displacements

Fig. 4 Measured geometric imperfections of columns in silo '2' in Poland

5. Simplified FE analyses of silo

5.1 Single column on elastic foundation

The initial FE calculations were carried out with 2 numerical models of columns: 1) composed of beam elements and 2) composed of shell elements. In the first case, 240 beam elements B31 were employed and in the second case 8000 4-node rectangular shell elements (ABAQUS 2010). The columns were fixed at the bottom. The stiffness of the elastic foundation provided by the corrugated sheet walls was calculated with Eq. (9). The first eigen-mode calculated from a linear buckling analysis (LBA) was chosen as the initial geometric imperfection. The Riks method

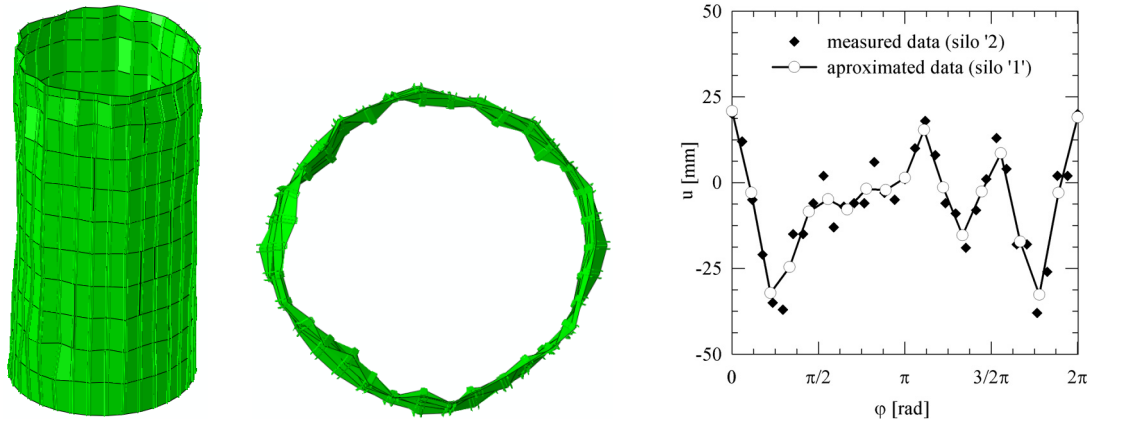

(a) General 3D view (b) Mid-cross-section (scale 20:1) (c) Approximation of measured displacement along silo circumference (φ - pole angle and u - horizontal displacement)

Fig. 5 Measured radial column displacements in empty cylindrical metal silo '2' (H = 29 m, D = 15.4 m) transferred to silo '1'

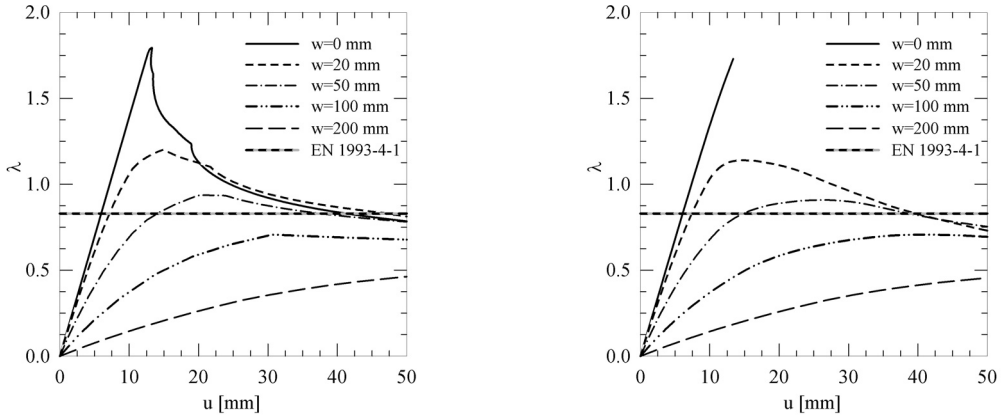

(a) Beam elements (b) Shell elements

Fig. 6 Non-linear static analyses GMNIA of single column on elastic foundation: evolution of load factor λ versus vertical column top displacement u against different horizontal amplitude w of initial geometric imperfection in form of first eigen-mode

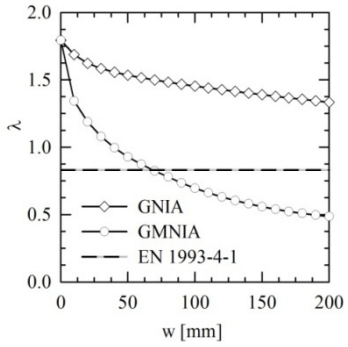

Fig. 7 Non-linear static analyses (GNIA and GMNIA) of single column on elastic foundation: limit load factor λ versus initial imperfection amplitude w for imperfection in form of first eigen-mode

(ABAQUS (2010)) with the automatic load increment was used to determine the force-deflection curve and load factor λ, defined as the ratio between the buckling wall pressure and wall pressure due to axisymmetric emptying (EN 1991-4 2006). The maximum force increment was taken as 5% of the total vertical force by EN 1991-4 2006.

Fig. 6 shows the influence of the horizontal imperfection amplitude on the load factor λ for 2 numerical models of a single column, i.e., with the beam and shell elements, as a function of the vertical displacement of the column top u for the different amplitudes w of the initial geometric imperfection (from LBA). The change of the limit load for the geometric non-linear analysis with the elastic (GNA) and perfectly-plastic material (GMNIA) is presented in Fig. 7. The imperfection amplitude in GMNIA had a significant influence on the column load. In the range of the maximum initial horizontal wall imperfection amplitude of w = 0-20 cm, the limit load factor λ was the same as for the column described with the beam or shell elements. The column resistance for w = 5-8 cm corresponded well to the buckling resistance following EN 1993-4-1 (2007) (λ = 0.83, Eq. (8)). The lowest load factor λ = 0.49 at w = 20 cm was by 73% lower than for the perfect column. The

limit load factor for the perfect column was $\lambda = 1.8$ and was equal to $N_{b,Rk(1)}/N_{b,Ek} = 1.8$ (profile C 4.0). The critical resistance $N_{b,Rk(2)}$ ($\lambda = 4.3$, Eq. (5)) was 2.4-times higher than the limit load for the perfect column in the non-linear FE analysis. The buckling resistance was the same in GNIA and GMNIA for the perfect column (Fig. 7). The minimum load factor in GNA at $w = 20$ cm was $\lambda = 0.83$ and was by 26 % lower than for the perfect column. The load factor in GNA was much less sensitive to imperfections than in GMNIA.

5.2 3D silo model with equivalent orthotropic shell

The full shell silo 3D FE model of corrugated sheets and thin-walled columns requires a huge amount of elements (see Section 5). In order to significantly reduce the computation time, a so-called equivalent orthotropic shell 3D model was used. The corrugated sheet wall panels were replaced by the orthotropic shell panels. The 3D FE buckling analysis of the entire silo structure was performed with a silo shell described by shell elements possessing equivalent properties as corrugated walls and with vertical columns represented by beam elements. The elastic constitutive equation of the equivalent orthotropic plate is (Xia *et al*. 2012)

$$\begin{bmatrix} N_x \\ N_y \\ N_{xy} \\ M_x \\ M_y \\ M_{xy} \end{bmatrix} = \begin{bmatrix} C_{11} & C_{12} & 0 & 0 & 0 & 0 \\ C_{12} & C_{22} & 0 & 0 & 0 & 0 \\ 0 & 0 & C_{33} & 0 & 0 & 0 \\ 0 & 0 & 0 & D_{44} & D_{45} & 0 \\ 0 & 0 & 0 & D_{45} & D_{55} & 0 \\ 0 & 0 & 0 & 0 & 0 & D_{66} \end{bmatrix} \times \begin{bmatrix} \varepsilon_x \\ \varepsilon_y \\ \varepsilon_{xy} \\ \kappa_x \\ \kappa_y \\ \kappa_{xy} \end{bmatrix}, \tag{11}$$

The full shell silo 3D FE model of corrugated sheets and thin-walled columns requires a huge amount of elements (see Section 5). In order to significantly reduce the computation time, a so-called equivalent orthotropic shell 3D model was used. The corrugated sheet wall panels were replaced by the orthotropic shell panels. The 3D FE buckling analysis of the entire silo structure was performed with a silo shell described by shell elements possessing equivalent properties as corrugated walls and with vertical columns represented by beam elements. The elastic constitutive equation of the equivalent orthotropic plate is (Xia *et al*. 2012)

$$C_{11} = Et_x = E\frac{2t^3}{3d^2}, \tag{12}$$

$$C_{22} = Et_y = Et\left(1+\frac{\pi^2 d^2}{4l^2}\right), \tag{13}$$

$$C_{12} = \nu C_{11}, \tag{14}$$

$$C_{33} = Gt_{xy} = \frac{Gt}{\left(1+\frac{\pi^2 d^2}{4l^2}\right)}, \tag{15}$$

$$D_{44} = EJ_x = \frac{Et^3}{12(1-\nu)} \cdot \frac{1}{\left(1+\frac{\pi^2 d^2}{4l^4}\right)}, \tag{16}$$

$$D_{55} = EJ_y = 0.13Etd^2, \tag{17}$$

$$D_{45} = \nu D_{44}, \tag{18}$$

$$D_{66} = GJ_{xy} = \frac{Gt^3}{12} \cdot \left(1+\frac{\pi^2 d^2}{4l^4}\right), \tag{19}$$

where E – the Young modulus, ν – the Poisson ratio, G – the shear modulus, l – the wall corrugation length, t – the plate thickness and d – the wall corrugation height.

The connection between columns and wall was assumed as fixed. The separated hopper and roof were neglected due to their an insignificant effect on results. The silo steel was assumed to be elastic-perfectly plastic. Two different element types (available in ABAQUS (2010)) were adopted to describe the columns: the usual Euler-Bernoulli beam elements (B33) with six degrees of freedom per node and the Timoshenko beam elements (B31OS) with one additional degree of freedom (in order to capture the element warping). The linear shape functions were used for B31OS elements and the cubic functions for B33. In order to describe the equivalent orthotropic plain shell silo mantle, the 4-node fully integrated shell element S4 and 4-node shell element with the reduced integration S4R were considered. The cylinder mesh for rectangular elements was divided into 18×6 = 108 elements in a circumferential direction and 120 elements in an axial direction.

The following 3 different analysis types were conducted:

(1) linear buckling analysis of a perfect silo (LBA),
(2) geometrically non-linear analysis of a perfect (GNA) and an imperfect silo (GNIA),
(3) geometrically and materially non-linear analysis of a perfect (GMNA) and an imperfect silo (GMNIA).

The linear and nonlinear analyses were performed for 3 various silo wall loads for determining the most detrimental initial geometric imperfections: (1) vertical wall friction stress ('V'); (2) vertical wall friction stress and horizontal wall pressure ('V+H'); and (3) vertical wall friction stress, horizontal normal wall pressure and patch wall load ('V+H+P'). The first silo eigen-mode from LBA and geodetic measurements were assumed as the initial geometric imperfections.

5.2.1 Linear buckling analyses (LBA)

The first buckling eigen-mode of a silo with shell elements S4 obtained from LBA for the different silo wall loads are presented in Fig. 8. The lowest buckling factor $\lambda = 5.5$ was for the wall load 'V' with a symmetric buckled form (Fig. 8(b)). The maximum deformation occurred in the lower silo-half. The buckled silo included 4 half-waves in a vertical direction and 18 half-waves in a circumferential direction (Fig. 8(b)). Assuming other wall loads, the silo deformations were concentrated near the bottom (Figs. 8(c)-(d)). For the wall load 'V+H', 3 half-waves in a vertical direction and 12 half-waves in a circumferential direction were calculated ($\lambda = 10.5$) (Fig. 8(c)).

The buckled form for the wall load 'V+H+P' was asymmetric and had 3 half-waves in a vertical direction and 5 half-waves in a circumferential direction (λ = 9.2) (Fig. 8(d)). The mesh size effect was negligible on the LBA results - smaller than 2% for a finer mesh. Surprisingly, the first eigen-mode of the silo described by the shell elements S4R (for the wall load 'V') indicated a spurious buckle forms for the load factor $\lambda < 1$. The LBA results showed that the fully integrated elements (S4) were the most suitable for calculations since they created an axisymmetric mesh and were not sensitive to spurious modes. They were used in further computations in this section.

5.2.2 Geometrically non-linear static analyses

The load increment in GNIA was set as 1% of the critical load from LBA. The results for two types FE elements (B31OS and B33) were similar but in many cases, the B33-element indicated the convergence lack at the low load level. The maximum load factor for the perfect silo was λ = 12.9 and was greater by 40% as compared to LBA.

Fig. 9 shows the diagrams of the load factor λ against the amplitude w of imperfections obtained from GNIA for the different wall load. The wall loads: 'V, 'V+H' and 'V+H+P' were the same as in linear buckling computations. Two types of initial imperfections were taken into account: 1) in the form of the 1-st buckling mode as in Section 4.1.1 (Fig. 8) and 2) based on the approximated geodetic measurements (Fig. 5).

The GNIA results (Fig. 9) showed that the silo with the only vertical load '*V*' was more sensitive to imperfections and had the lowest buckling strength (λ = 1.8-4.3). In the range of the amplitude w = 0-5 cm (Fig. 9(a)), the limit load factor, λ = 4, was by 27% lower than in LBA, and for w = 20 cm the load factor was λ = 1.8 and was by 67% lower than in LBA.

For the silo with the imperfection from LBA (Fig. 8) and wall loads '*V+H*' and '*V+H+P*', the change of the limit load factor was similar for the range w = 0-5 cm (λ = 8-8.5), but for the range w = 5-20 cm some differences occurred (Fig. 9(a)). The curve shape was generally smooth (Fig. 9(a)).

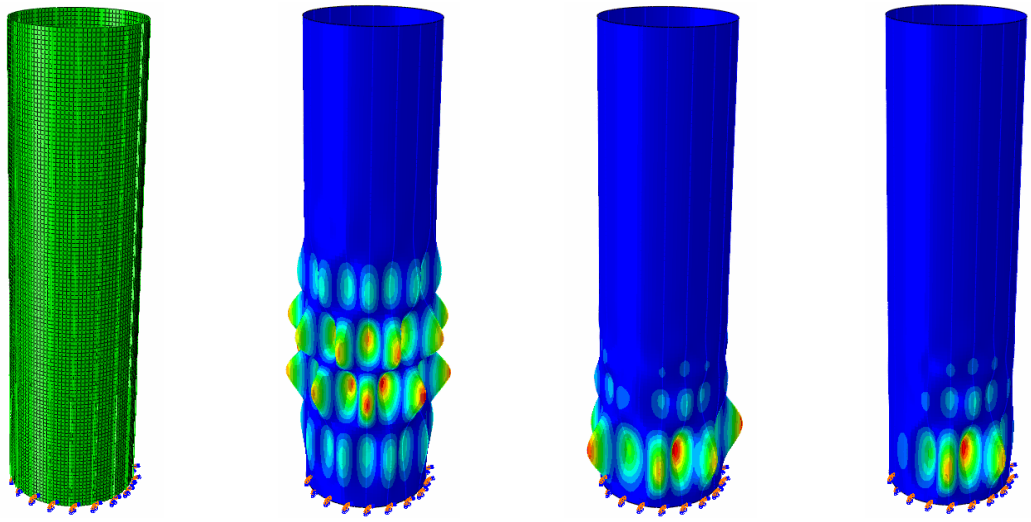

(a) FE mesh (b) '*V*' (λ = 5.5) (c) '*V+H*' (λ = 10.5) (d) '*V+H+P*' (λ = 9.2)

Fig. 8 First buckling mode (LBA) of silo model with equivalent orthotropic mantle and external columns subjected to different wall load ('*V*' – frictional traction, '*H*' - normal horizontal wall pressure and '*P*' - patch load) and the calculated load factor

The limit load factor for w = 20 cm (λ = 6.9) was by about 25% lower than in LBA (λ = 9.2). For the measured imperfections, the limit load factor for the wall loads '*V+H*' and '*V+H+P*' (λ = 7-10) was more random (Fig. 9(b)). The silo with the vertical wall load ('*V*') had a higher buckling resistance in the entire range of w = 0-20 cm than with the imperfection from LBA.

Note that EN 1993-4-1 (2007) estimates a negative effect of imperfections in Eq. (5) by introducing the constant α_x = 0.8 which corresponds well with GNIA results.

The presence of the horizontal wall load '*H*' had a significant positive influence on the silo strength. The silo with the wall loads '*V+H*' and '*V+H+P*' had the about 2-3-times higher the limit load factor than the silo with the vertical load '*V*'. The effect of the patch load '*P*' was negative for the silo stability, however its effect was rather marginal (Fig. 9), especially for a silo with initial imperfections based on geodetic measurements.

Figs. 10-11 presents the load factor λ against the vertical displacement u of the silo top for 4 different imperfection amplitudes (w =2 0, w = 50, w = 100 and w = 200 mm). In some cases the silo after a first bifurcation point had a stable behaviour (Fig. 10(b)). The post-critical solutions in many numerical cases were not obtained due to some convergence problems. Figs. 10-11 show that the relationship λ-u before the first instability was more linear for the geodetic initial imperfections. In general, the silo stiffness after each critical point decreased.

5.2.3 Geometrically and materially non-linear static analyses

The silo buckling resistance for the perfect silo was λ = 2.3. Fig. 12 presents the change of the limit load factor as the function of the imperfection amplitude w for 2 different shapes of the initial deformation. The highest influence of the initial imperfections on the ultimate load induced by the different wall load (Fig. 12) was observed for the 'V'-load. Fig. 12(b) shows that for the different loads and the same shape of the initial imperfection, the effect of the patch load is negligible. The silo ultimate loads were significantly smaller than in the calculations of GNA and GNIA (λ = 2-12). Comparing with EN 1993-4-1 (2007), the limit load for the perfect silo was by 30% higher than $N_{brk,1}$ (Eq. (6)), by 45% lower than $N_{brk,2}$ (Eq. (5)) and by 180% higher than $N_{brk,3}$ (Eq. (8)).

The load factor-vertical displacement curves obtained from geometrically and materially non-linear analyses were obviously different as compared to analyses without the material non-linearity because of the occurrence of plastic deformations (Figs. 13 and 14).

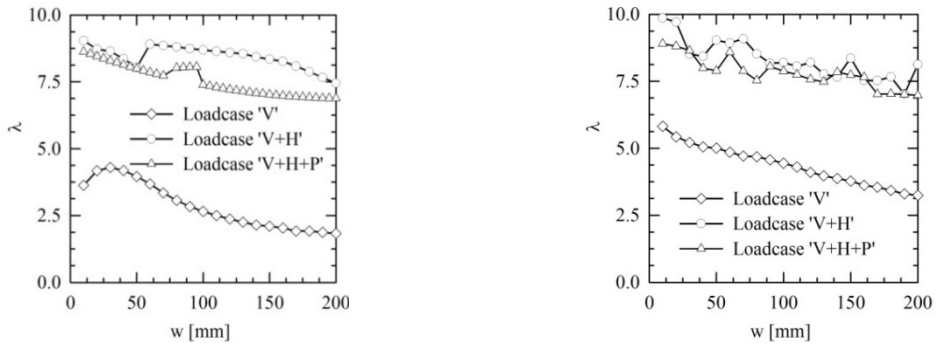

(a) Imperfection shape: 1-st eigen-mode (LBA) (b) Imperfection shape: geodetic measurements

Fig. 9 Change of limit load factor λ against various amplitude of initial imperfection w (non-linear static analyses GNIA for silo model with equivalent orthotropic shell with different shape of initial imperfections and different wall load)

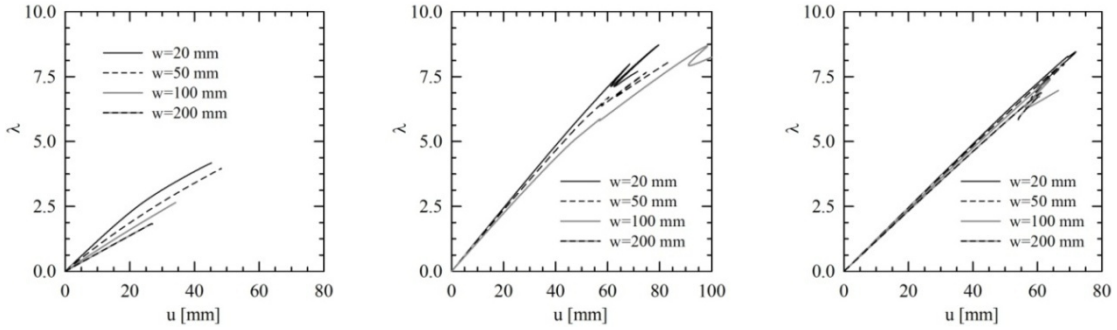

(a) wall load: 'V' (b) wall load: 'V+H' (c) wall load: 'V+H+P'

Fig. 10 Change of limit load factor λ against vertical top column displacement u (non-linear static analyses GNIA for silo model with equivalent orthotropic shell and initial imperfections (1-st buckling mode from LBA) subjected to different wall load

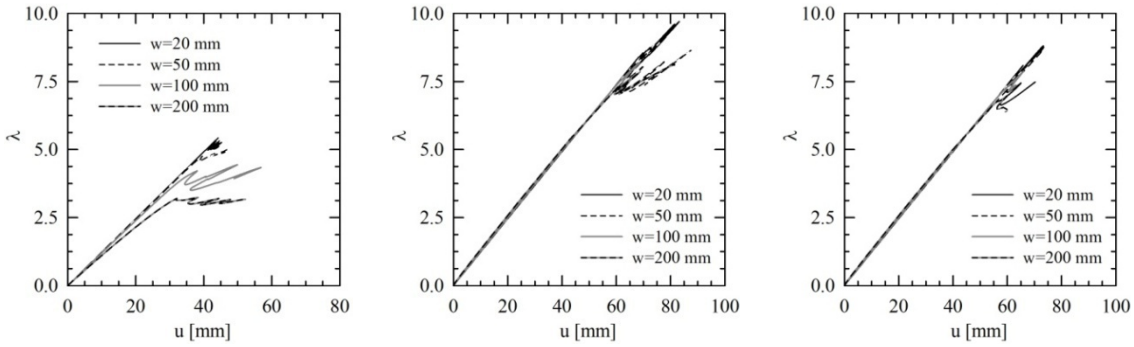

(a) Wall load: 'V' (b) Wall load: 'V+H' (c) Wall load: 'V+H+P'

Fig. 11 Change of limit load factor λ against vertical top column displacement u (non-linear static analyses GNIA for silo model with equivalent orthotropic shell and initial imperfections (geodetic measurements) subjected to different wall load

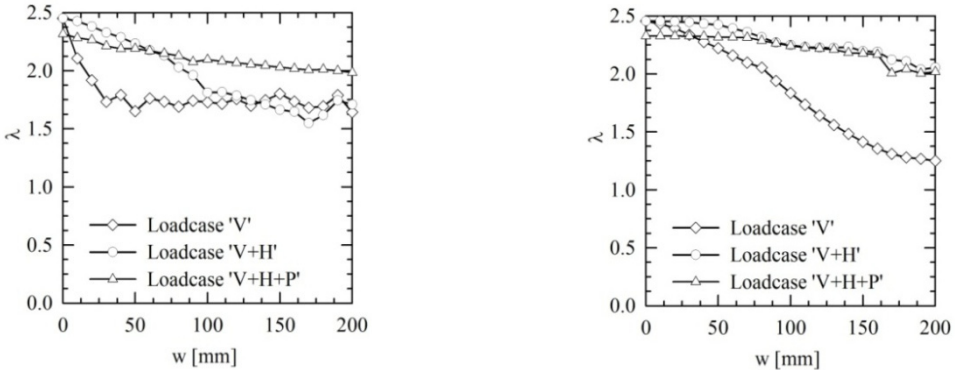

(a) Imperfection shape: 1-st eigen-mode (LBA) (b) Imperfection shape: geodetic measurements

Fig. 12 Limit load factor λ for different amplitudes of initial imperfection w (non-linear static analyses GMNIA for silo model with equivalent orthotropic shell with different shapes of initial imperfections and wall load

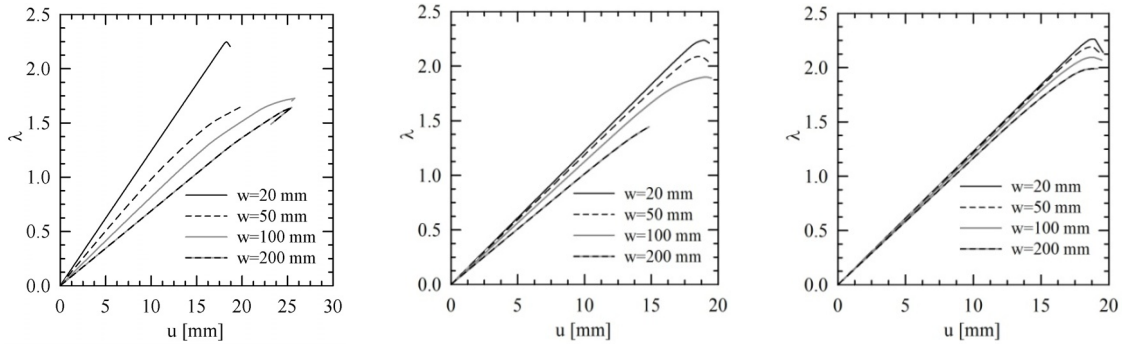

(a) Wall load: 'V' (b) Wall load: 'V+H' (c) Wall load: 'V+H+P'

Fig. 13 Change of limit load factor λ against vertical top column displacement u (non-linear static analyses GMNIA for silo model with equivalent orthotropic shell and initial imperfections (1-st buckling mode from LBA) subjected to different wall load

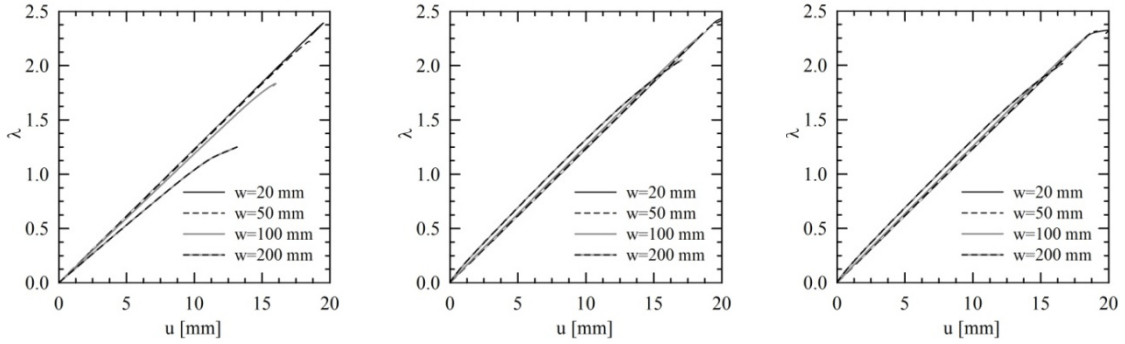

(a) Wall load: 'V' (b) Wall load: 'V+H' (c) Wall load: 'V+H+P'

Fig. 14 Change of limit load factor λ against vertical top column displacement u (non-linear static analyses GMNIA for silo model with equivalent orthotropic shell and initial imperfections (geodetic measurements) subjected to different wall load

6. Full 3D silo model with shell elements

The FE linear and non-linear stability calculations of a silo with corrugated wall sheets and thin-walled column profiles were performed for the same load and boundary conditions as the previous studies (Section 4). The silo geometry slightly differed from the previous FE models. The cross-sectional centre line for all 'C' profiles were assumed to be the same as for the C1.5 (Fig. 1). Due to this simplification the limit loads were by about 10% smaller than for the real geometry. The corrugated walls were fixed to the columns at the sheet wave top at a constant distance of 0.076 m. In order to describe the corrugated walls and columns, the 4-node shell elements S4R were employed (ABAQUS 2010). The preliminary FE simulations showed that these elements did not indicate spurious forms (in contrast to the results in Section 4) and provided the same results as with the S4 elements. The total amount of finite elements of the finest silo mesh was huge, i.e., 3.7 millions with the smallest shell element of corrugated sheets 5×19 mm^2 and columns 10×10 mm^2.

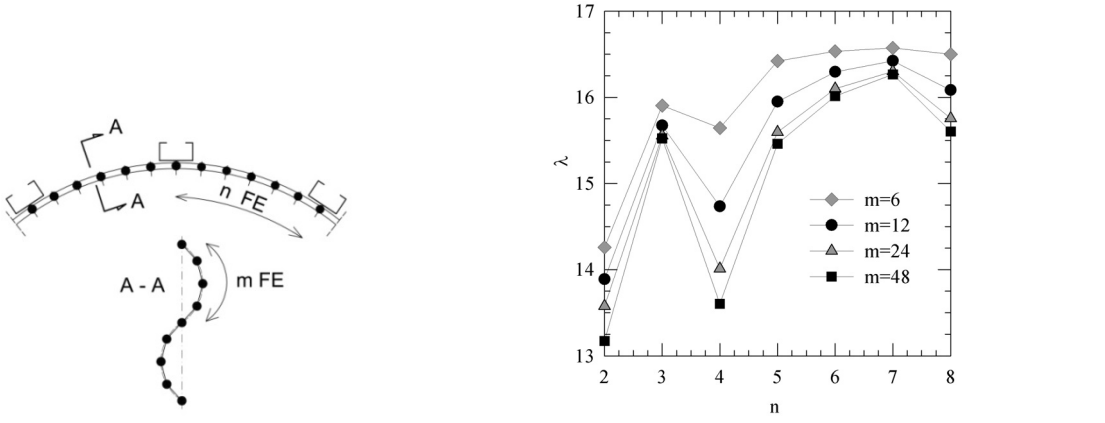

(a) Discription of *n*- and *m*-number

(b) Buckling load factor λ against element number *n* along corrugated wave for different number of *m*-elements between columns

Fig. 15 Effect of mesh discretization on load factor λ (LBA)

Two kinds of initial geometrical imperfections were again taken into account: (a) equal to the first eigen-mode from LBA; and (b) based on the geodetic measurements.

6.1 Initial imperfections from linear buckling analyses (LBA)

The linear buckling analysis was performed with the 10-times higher modulus of elasticity of columns in order to suppress their local buckling and with the vertical wall load '*V*' to avoid the local buckling of corrugated wall sheets. The FE discretization significantly affected the shape of the first buckling mode. The buckled forms for the coarse meshes (2 and 3 elements along the wall half-wave) included the 14 half-waves along the circumference and were non-symmetric. The buckled forms for the meshes with the minimum 4 elements along the wall half-wave had the 12 half-wave along the circumference and were less non-symmetric. An increase of the element amount along the vertical and a decrease of the element number along the silo circumference contributed to a higher limit load factor λ from λ = 13.2-15.6 up to λ = 14.3-16.5 (Fig. 15(b)). The maximum difference of the buckling load factor λ for all analysed meshes was about 25%. Fig. 15(b) shows that the element numbers (n = 3 and m = 6) were sufficient for this silo to realistically predict the buckling load factor.

6.2 Geometrically and materially non-linear stability analyses

The silo failure (Fig. 16) was always initialized by some local plastic regions located at junctions of two different column profile (C4.0 and V4.0 (Fig. 1)) The limit load factor with the measured geometric imperfections of Fig. 5 was higher than this with the imperfections in the form of a first buckling shape-mode from LBA (with the vertical wall friction load). For w = 5 cm (the maximum measured horizontal amplitude) it was higher by 12%. For w = 5 cm, the limit load factor, λ = 2.0, was significantly higher than in a numerical model of a single column on the elastic foundation, λ = 0.83 (Eq. (8)) and slightly lower than for a silo with the equivalent orthotropic shell of Section 4 (λ = 2.3).

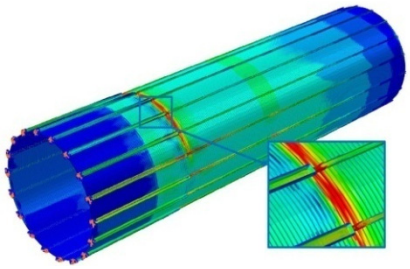

Fig. 16 Calculated deformed silo shell with von Mises stresses for perfect silo during local plastic-buckling from geometrically and materially nonlinear buckling analyses (full 3D silo model)

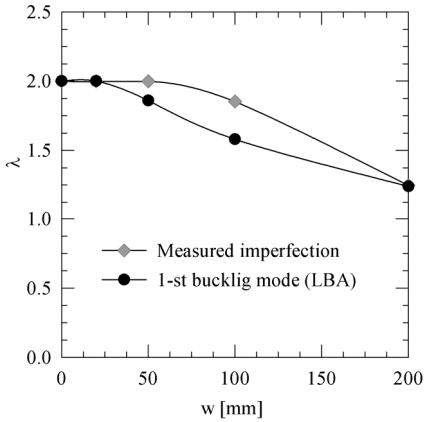

Fig. 17 Limit load factor λ against initial imperfection amplitude w (full 3D silo model, GMNIA) for 2 different imperfections: from measurements (Fig. 5) and first buckling shape-mode from LBA

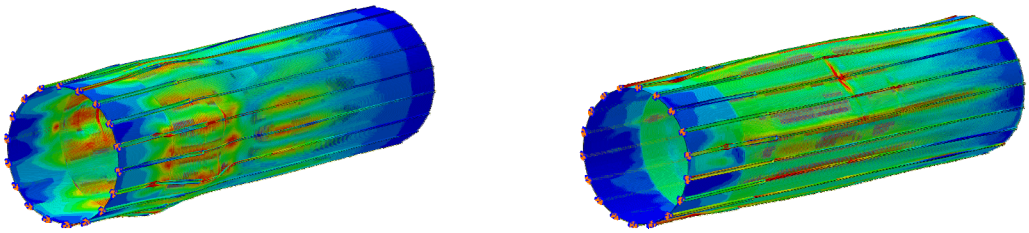

(a) First buckling shape-mode from LBA (b) From measurements

Fig. 18 Deformed silo shape from non-linear analysis GMNIA for initial imperfection amplitude w = 20 cm (full 3D silo model) for 2 different imperfection types

The local yield stress of 350 MPa appeared before the buckling load factor from LBA was achieved. In the range of w = 0-5 cm, the silo deformations were similar for the both shapes of initial imperfections, i.e., the profile junctions 'C' and 'V' were found to be the weakest (the first local yield stress occurred for the load factor already for λ = 1.0, Fig. 16). The plastic deformation in corrugated wall sheets was observed in a post-buckling stage only independently of the imperfection type (Fig. 18).

The major differences in the stability strength of the silo FE models occurred at w = 20 cm, where some local effects became of a major importance. The lowest limit load factor was obtained for a single column supported by the elastic foundation and the highest for the FE model with equivalent orthotropic shell and beam elements.

7. Conclusions

The following conclusions can be derived from our stability analyses for cylindrical metal silos with corrugated sheets and open-sectional column profiles:

- The strongly simplified FE model of a silo column supported by the elastic foundation without initial imperfections estimates a global buckling strength on a very safe side. The calculated limit load factor with the initial imperfection amplitude range w = 6-8 cm corresponds to the limit load factor following Eurocode 3 (λ = 0.83, Eq. (80). If a local stability occurs, this model obviously overestimates the strength.
- The most realistic stability strength and buckling form are determined based on non-linear analyses of a silo modelled completely with shell elements (S4R) by assuming geometric and material non-linearity. The numerical model is able to capture the both global and local buckling failure type. Some convergence problems are met during both geometrically and materially non-linear static analyses. The mesh discretization of columns is crucial for the buckling strength. The smaller the element size in columns, the lower is the stability strength. The effect of the mesh density of the corrugated wall sheets was observed in linear buckling analyses only. The appropriate buckling strength results may be already achieved using 3 shell elements along the half-wave and 6 shell elements in a circumferential direction between columns and column elements 10×10 mm^2.
- The simplified silo model with the equivalent orthotropic plate and beam columns turns out to be effective to assess the stability using the fully integrated shell elements (S4). The limit load is comparable with a complex full shell silo model. The beam model is thus sufficient for the stability analyses when thin-walled columns are insensitive to local buckling effects. The computations time is significantly shorter (2-5-times) than for the full 3D silo model.
- Due to a specific assembly method of silos with corrugated sheets and thin-walled columns, the measured imperfection pattern significantly differs from those assumed in FE models based on eigen-modes from LBA. It is recommended to model the assembly process in order to obtain realistic initial geometric imperfections.
- The initial geometric imperfections may be taken in the form of a first eigen-mode since the strength of a shell silo model is smaller solely by 0-20% than of the silo with measured imperfections (although its form is completely different). It is recommended to introduce into FE analyses initial geometric imperfections in the form of the first silo eigen-mode induced by wall friction (with eventually stiffened columns) for the maximum amplitude of w = 5 cm in order to provide a sufficient safety margin for the silo design.
- The EN 1993-4-1 (2007) approach based on a beam supported by the elastic foundation (Eq. (8)) is not realistic. The formulae for 2 alternative standard approaches are not continuous. Eq. (8) is significantly too conservative if d_s is small. It is reasonable to use a FE analysis especially in the case of $d_s < d_{s,\max}$.

- The buckling resistance in EN 1993-4-1 (2007) based on an anisotropic cylinder theory (Eq. (5)) is in good agreement with FE results for a silo with the equivalent orthotropic shell with the vertical wall load 'V' in the range of the imperfection amplitude w = 0-5 cm.

The normal wall pressure has a significant positive influence for the silo stability.

Acknowledgments

The financial support of the Polish National Research Centre NCN in the frame of the Grant 2011/01/B/ST8/07492 "*Safety and optimization of cylindrical metal silos containing bulk solids with respect to global stability*" and of the Polish National Applied Research Centre NCBR in the frame of the Grant POIG.01.03.01-00-099/12 "*Innovative method of dimensioning and construction of large industrial silos made from of corrugated sheets*" is gratefully acknowledged.

References

ABAQUS (2010), ABAQUS Documentation, Dassault Systèmes Simulia Corp., Providence, RI, USA.

Brown, C.J. and Nielsen, J. (1998), *Silos – Fundamentals of Theory*, *Behavior and Design*, E and FN Spon., London, UK.

EN 1991-4 (2006), Eurocode 1: Actions on structures. Part 4: Silos and tanks; CEN, Brussels, Belgium.

EN 1993-1-3 (2006), Eurocode 3: Design of Steel Structures. Part 1-3: General rules - Supplementary rules for cold-formed members and sheeting; CEN, Brussels, Belgium.

EN 1993-4-1 (2007), Eurocode 3: Design of Steel Structures. Part 4-1: Silos; CEN, Brussels, Belgium.

Fayed, N. and Otten, L. (1997), *Handbook of Powder Science and Technology*, (2nd ed.), Chapman and Hall, New York, NY, USA.

Gallego, E., González-Montellano, C., Ramírez, A. and Ayuga, F. (2011), "A simplified analytical procedure for assessing the worst patch load location on circular steel silos with corrugated walls", *Eng. Struct.*, **33**(6), 1940-1954.

Iwicki, P., Wójcik, M. and Tejchman, J. (2011), "Failure of cylindrical steel silos composed of corrugated sheets and columns and repair methods using a sensitivity analysis", *Eng. Fail. Anal.*, **18**(8), 2064-2083.

Iwicki, P., Tejchman, J. and Chróścielewski, J. (2014), "Dynamic FE simulations of buckling process in thin-walled cylindrical metal silos", *Thin-Wall. Struct.*, **84**, 344-359.

Knebel, K. and Schweizerhof, K. (1995), "Buckling of cylindrical shells containing granular solids", *Thin-Wall. Struct.*, **23**(1-4), 295-312.

Kobayashi, T., Mihara, Y. and Fujii, F. (2012), "Path-tracing analysis for post buckling process of elastic cylindrical shells under axial compression", *Thin- Wall. Struct.*, **61**, 180-187.

Kubiak, T. (2007), "Criteria of dynamic buckling estimation of thin-walled structures", *Thin- Wall. Struct.*, **45**(10-11), 888-892.

Rotter, J.M. (2001), *Guide for the Economic Design of Circular Metal Silos*, Spon Press, New York, NY, USA.

Sadowski, A.J. and Rotter, J.M. (2011), "Buckling of very slender metal silos under eccentric discharge", *Eng. Struct.*, **33**(4), 1187-1194.

Safarian, S.S. and Harris, E.C. (1985), *Design and Construction of Silos and Bunkers*, Van Nostrand Reinhold Company, New York, NY, USA.

Song, C.Y. and Teng, J.G. (2003), "Buckling of circular steel silos subjected to code-specified eccentric discharge pressures", *Eng. Struct.*, **25**(11), 1397-1417.

Tejchman, J. (1999), "Technical concept to prevent the silo honking", *Powder Technology*, **106**(1-2), 7-22.

Tejchman, J. and Gudehus, G. (1993), "Silo-music and silo-quake, experiments and a numerical Cosserat approach", *Powder Technology*, **76**(2), 201-212.
Wilde, K., Rucka, M. and Tejchman, J. (2008), "Silo music - Mechanism of dynamic flow and structure interaction", *Powder Technology*, **186**(2), 113-129.
Wójcik, M., Iwicki, P. and Tejchman, J. (2011), "3D buckling analysis of a cylindrical metal bin composed of corrugated", *Thin-Wall. Struct*., **49**(8), 947-963.
Xia, Y. Friswell, M.I. and Saavedra Flores, E.I. (2012), "Equivalent models of corrugated panels". Internat. *J. Solid. Struct*., **49**(13), 1453-1462.

CC